

The Shapes of Elliptical Galaxies with Central Density Cusps and Massive Dark Objects

Barbara S. Ryden,¹

Department of Astronomy, The Ohio State University, 174 W. 18th Avenue, Columbus, OH 43210

ABSTRACT

For a sample of 22 core ellipticals, with shallow central cusps, and 22 power law ellipticals, with steep central cusps, I examine the apparent axis ratios of isophotes as a function of the dynamical time at the isophote's mean radius. The two types of elliptical galaxy have a significantly different distribution of shapes in the region where the dynamical time is short (~ 1 Myr); the core galaxies are rounder in this region. In the outer regions ($t_{\text{dyn}} \gtrsim 10$ Myr), the two types have indistinguishable shape distributions. I perform a more detailed analysis of the apparent and intrinsic shapes at two chosen locations: an inner region, where $t_{\text{dyn}} = 0.75$ Myr, and an outer region, where $t_{\text{dyn}} = 50$ Myr. The inner isophotes of core galaxies are consistent with their being randomly oriented oblate objects, with a peak intrinsic axis ratio of $\gamma = 0.86$. The outer regions of core galaxies are inconsistent with their being randomly oriented oblate or prolate objects, at a 99% confidence level. The oblate hypothesis cannot be rejected for the inner and outer regions of power law galaxies at the 90% confidence level; however, if power law galaxies are oblate, very few of them can be nearly spherical, with $\gamma > 0.8$. The observed shapes are consistent with the hypothesis that the inner regions of core galaxies are nearly spherical and nearly axisymmetric, perhaps as the result of the physical process which formed the core.

Subject headings: galaxies: elliptical and lenticular, cD – galaxies: structure

1. Introduction

A growing body of evidence (as outlined, for instance, by Kormendy & Richstone 1995) indicates that elliptical galaxies typically harbor a central massive dark object (or MDO). The masses of MDOs in elliptical galaxies are best determined for giant ellipticals with nuclear gas disks, such as M87 (Harms et al. 1994), NGC 4261 (Ferrarese, Ford, & Jaffe 1996), and M84

¹National Science Foundation Young Investigator; ryden@astronomy.ohio-state.edu.

(Bower et al. 1998). Stellar dynamics can also yield estimates for MDO masses, although the estimated masses are model-dependent. For example, Magorrian et al. (1998) looked at a sample of nearby galaxies with *Hubble Space Telescope (HST)* photometry and ground-based kinematics. Of the 32 elliptical galaxies in their sample, they found that 28 were well fitted by an axisymmetric model with a two-integral distribution function, a constant mass-to-light ratio, and an optional MDO. Of the galaxies consistent with their model, 26 required the presence of an MDO for the best fit, with a typical MDO mass of $M_{\bullet} \sim 0.005M_{\text{gal}}$, where M_{gal} is the mass of the stellar component of the galaxy.

In addition to housing central MDOs, most elliptical galaxies have central cusps in the luminosity density $\nu(r)$. For a sample of early-type galaxies observed by *HST* (Gebhardt et al. 1996), the logarithmic slope of the luminosity density, $\eta \equiv -d \log \nu / d \log r$, is significantly different from zero for most galaxies at $0.1''$ from the galaxy center. Elliptical galaxies fall into two distinct classes, distinguished by their central density profile (Jaffe et al. 1994, Lauer et al. 1995); “core” galaxies have shallow cusps, with $\eta \sim 0.8$, and “power law” galaxies have steeper cusps, with $\eta \sim 1.9$ (Gebhardt et al. 1996).

The presence of a central MDO or density cusp has a significant effect on the structure of an elliptical galaxy (Gerhard & Binney 1985, Norman et al. 1985). In particular, it determines whether or not a galaxy can be highly triaxial. (The phrase “highly triaxial” can be quantified. Consider an ellipsoid with principal axes of length $a \geq b \geq c$. The triaxiality is customarily given by the parameter $T \equiv (1 - b^2/a^2)/(1 - c^2/a^2)$. An ellipsoid with $T \approx 0$ is nearly oblate, an ellipsoid with $T \approx 1$ is nearly prolate, and an ellipsoid with $T \approx 1/2$ is highly triaxial.) In a stellar system with a constant density core, such as the “perfect ellipsoid” (Kuzmin 1956, de Zeeuw 1985), stars can follow box orbits, on which stars eventually come arbitrarily close to the center, or tube orbits, on which stars circulate about the long or short axis of the system. Box orbits are generally referred to as the “backbone” of a triaxial galaxy; since tube orbits can only be used to construct a nearly axisymmetric system, the presence of box orbits is required for a highly triaxial system. However, in a galaxy with a central point mass or a steep density cusp, box orbits are broken up; a star on a box orbit will eventually have a close encounter with the central mass, subjecting the star to a large-angle deflection.

Modeling galaxies with density cusps, $\rho \propto r^{-\eta}$, places restrictions on their permitted equilibrium shapes. Schwarzschild (1993) examined self-similar triaxial models with $\eta = 2$; he discovered that self-consistent models were not possible for extremely flattened galaxies ($c/a = 0.3$). In his highly flattened triaxial models, Schwarzschild found that many of the orbits were stochastic, changing shape significantly over ~ 160 orbital times. Merritt & Fridman (1996) found that for weak cusps, with $\eta = 1$, as well as for strong cusps, with $\eta = 2$, a large fraction of model orbits are stochastic. The mixing time in phase space for the stochastic orbits is roughly 100 times the orbital period for a model with a steep cusp, but may be more than 1000 times the orbital period for a model with a weak cusp.

Since stochastic orbits in a triaxial potential are nearly axisymmetric and nearly spherical, it is impossible to create an equilibrium self-consistent model for a strongly triaxial galaxy with a central density cusp. For a Jaffe model, which has $\eta = 2$ in the central regions, Merritt (1997) found self-consistent solutions only for models which were both nearly axisymmetric ($T \lesssim 0.4$ or $T \gtrsim 0.9$) and nearly spherical ($c/a \gtrsim 0.8$). Looking at models with different values of η , Fridman & Merritt (1997) found that cuspy models with $\eta \gtrsim 0.8$ can only have stable boxlike orbits if they are nearly spherical ($c/a \gtrsim 0.75$). Studies of scale-free, cuspy disks, with $c/a \rightarrow 0$, place severe restrictions on the shapes of highly flattened galaxies (Kuijken 1993; Syer & Zhao 1998); generally speaking, a cuspy galaxy in equilibrium cannot be both highly flattened and highly triaxial.

Central point masses are even more effective than central density cusps at inducing chaotic mixing of orbits. A relatively modest central black hole, with $M_{\bullet}/M_{\text{gal}} \approx 0.005$, is as effective as a steep $\eta = 2$ cusp at inducing chaotic mixing of orbits (Valluri & Merritt 1998). Numerical simulations (Merritt & Quinlan 1998) indicate that a black hole of this mass will change the galaxy’s overall shape on a time scale ~ 100 times the orbital period at the half-mass radius.

Observed elliptical galaxies have a range of cuspiness, as expressed by the logarithmic slope η of the luminosity density, and a range of MDO masses, as expressed by the ratio $x \equiv M_{\bullet}/M_{\text{gal}}$ of the MDO mass to the total stellar mass of the galaxy. Moreover, cuspiness and MDO mass appear to be inversely linked. In the sample of early-type galaxies modeled by Magorrian et al. (1998), the 21 core galaxies have a median $x = 0.0072$, and the 11 power law galaxies have a median $x = 0.0033$. Moreover, three of the power law galaxies, but none of the core galaxies, are best fit by a model with $x = 0$. A Kolmogorov-Smirnov (KS) test reveals that the distributions of x for the two populations differ at the level $P_{\text{KS}} = 0.014$.

Core ellipticals and power law ellipticals are known to differ in many properties other than the slopes of their density cusps. In addition to having steeper cusps and lower mass MDOs, power law ellipticals tend to have relatively low luminosity ($M_V > -22$), disk isophotes, and rapid rotation. Core ellipticals have relatively high luminosity ($M_V < -20.5$), boxy or elliptical isophotes, and slow rotation. The two classes also seem to differ systematically in their apparent axis ratios; Tremblay & Merritt (1996) showed that bright elliptical galaxies (which tend to be core galaxies) are rounder on average than fainter ellipticals. The shapes of the fainter ellipticals are consistent with their being randomly oriented oblate spheroids, but the bright ellipticals cannot all be oblate.

Tremblay & Merritt (1996) looked at the average shape of elliptical galaxies, represented by the luminosity-weighted axis ratio (Ryden 1992). In addition to looking at the average shape, it is also interesting to examine how the apparent shape of a galaxy’s isophotes changes with radius. For instance, consider an elliptical galaxy which is initially highly triaxial. (This is not an absurd assumption; the merger of two disk galaxies, for example, is capable of producing a highly triaxial remnant [Barnes 1992].) The central cusp and MDO of the elliptical galaxy will make it more nearly axisymmetric and more nearly spherical, starting from the inner regions, where the

dynamical time is shortest, and working steadily outward. If the characteristic time for changing the shape is $\sim 100t_{\text{dyn}}$, then at a given galaxy age t_{gal} , the inner region where $t_{\text{dyn}} < t_{\text{gal}}/100$ will be nearly axisymmetric and nearly spherical, while the outer regions will still retain their initial shape.

Is this naive picture true? Are real elliptical galaxies more nearly axisymmetric and spherical in their inner regions than in their outer regions? Does the variation of shape with radius differ for core galaxies and for power law galaxies? To investigate these questions, I examine the apparent shapes, as a function of isophotal radius, for a sample of nearby elliptical galaxies. The details of the galaxy sample used are given in Section 2 below. In section 3, I compare the shapes of the core galaxies and of the power law galaxies in the sample. For each galaxy, I compute the axis ratio of the isophote where the dynamical time is $t_{\text{dyn}} \sim 0.75$ Myr, and that of the isophote is $t_{\text{dyn}} \sim 50$ Myr. Comparing the inner isophotes, where the dynamical time is short, I find that the core galaxies are significantly rounder than the power law galaxies. At the outer isophotes, the core galaxies and power law galaxies have the same distribution of apparent shapes. In section 4, I summarize the results and their implications.

2. Galaxy Sample

The sample consists of 44 elliptical galaxies drawn from the study of Faber et al. (1997; hereafter F97), who compiled early-type galaxies that had been imaged by the *HST* Planetary Camera through filter F555W (approximately the *V* band). My sample of 44 ellipticals excludes NGC 7768, but includes every other galaxy in the F97 compilation which is classified as an E galaxy in the *Second Reference Catalog of Bright Galaxies* (de Vaucouleurs et al. 1976). NGC 7768 was excluded from the sample because its central dust disk strongly affects the surface brightness at *V* within about $0.4''$ of the galaxy’s center (Grillmair et al. 1994).

Although NGC 7768 was the only galaxy discarded from the sample due to the presence of dust, many of the remaining ellipticals contain detectable amounts of dust in their central regions (van Dokkum & Franx 1995), usually within a kiloparsec or so of the galaxy’s center. Thus, the effect of dust on isophote shapes is a potential concern when determining the shapes of the central regions of ellipticals. Some information on the effect of dust on the central isophote shapes comes from the study of Carollo et al. (1997); during their study of elliptical galaxies with kinematically distinct cores, they obtained *HST* WFPC2 images at F555W and F814W (roughly *V* and *I*) for 5 of the elliptical galaxies in the F97 sample: NGC 1700, NGC 3608, NGC 4365, NGC 4552, and NGC 5813. From their *V* and *I* images, Carollo et al. created “dust-improved” images that minimized, but did not eliminate, the effects of dust absorption. A comparison of the isophote parameters of the dust-improved images of Carollo et al. (1997) with the “unimproved” *V* images used by Faber et al. (1997) indicates no systematic difference between the isophote axis ratios in the central $2.5''$ of the images (Carollo et al. 1997). Speaking more generally, observed circumnuclear dust features in early-type galaxies are usually patchy, asymmetric, and/or

misaligned with the galaxy’s major axis (van Dokkum & Franx 1995). Features of this sort cause significant deviations from pure elliptical isophotes, as measured by the 3θ and 4θ terms in the Fourier expansion of the isophotes (Peletier et al. 1990), but do not strongly affect the measured axis ratio of isophotes. Because of the relative insensitivity of axis ratios to the presence of dust, I will use the published isophotal data for the F97 galaxies at face value, making no corrections for dust.

Over two-thirds of the galaxies in the F97 compilation are taken from the study of Lauer et al. (1995; hereafter L95). Lauer et al. were concerned with the central structure of nearby early-type galaxies. The elliptical galaxies in their sample span a broad range of luminosity, from the brightest cluster galaxy NGC 6166 ($M_V = -23.5$) to the M32 analog VCC 1199 ($M_V = -15.2$). The majority of the galaxies in the L95 sample were selected because ground-based photometry failed to resolve a central core. The L95 sample, and hence the F97 compilation, is weighted toward galaxies with high central surface brightness. The results which I derive in the present paper, therefore, are inapplicable to low surface brightness galaxies.

Of the 44 elliptical galaxies in the F97 sample, 22 are classified as core galaxies and 22 are classified as power law galaxies. The core subsample is listed in Table 1, and the power law subsample is listed in Table 2. For 35 of the galaxies, the isophotal parameters derived from the *HST* data are given by Lauer et al. (1995); these galaxies are indicated by the label ‘L95’ in the ‘inner isophote’ column of Tables 1 and 2. For 5 of the galaxies, the isophotal parameters are given by van den Bosch (1994); these are indicated by the label ‘V94’ in Tables 1 and 2. The isophotal parameters for NGC 4486 [M87] are given in Lauer et al. (1992; hereafter L92) and the parameters for NGC 221 [M32] are given by Lauer et al. (1998; hereafter L98). For NGC 1600, NGC 3379, NGC 4552, NGC 4621, and NGC 4649, isophotal parameters were provided in advance of publication (Lauer et al. 1999; hereafter L99).

The *HST* photometry for the galaxies in the sample includes roughly the central 10 arcsec of each galaxy, equivalent, at the distance of the Virgo cluster, to a linear scale of about 800 parsecs and a dynamical time, for a bright elliptical galaxy, of a few million years. To find the shapes of the outer regions of the galaxies, where the dynamical time is longer, I used isophotal parameters drawn from the published literature. For 17 galaxies, the outer isophotal parameters were taken from the work of Capaccioli and collaborators (Capaccioli et al. 1988, hereafter C88; Caon et al. 1990, hereafter C90; Caon et al. 1994, hereafter C94). These studies (C88, C90, & C94) combine CCD and photographic photometry in the B band to derive ellipticity and luminosity profiles to a limiting surface brightness of $\mu_B \sim 28 \text{ mag arcsec}^{-2}$; the ground-based B profiles were matched to the *HST* V profiles assuming a constant $B - V$ color outside the region imaged by *HST*. For an additional 12 galaxies, the outer isophotal parameters were taken from Peletier et al. (1990), who obtained CCD surface photometry for a selection of nearby bright ellipticals; they derived ellipticity and luminosity profiles in the R band and luminosity profiles in the B band to a limiting surface brightness of $\mu_B \sim 26 \text{ mag arcsec}^{-2}$. I computed an approximate V band profile by setting $V = (B + R)/2$, then adjusted the zero point to match the outermost isophote of the

published *HST* profile. Since the observed axis ratios of elliptical galaxies do not vary significantly with color (Peletier et al. 1990), I used the *R* band ellipticities as my measure of outer isophote shape. I drew additional ground-based data from other published sources, as listed in the “Outer isophotes” column of Tables 1 and 2. When the ground-based photometry was not in the *V* band, I assumed that the galaxy’s color in the outer regions was constant, with a value equal to the color at the outermost published *HST* isophote. I also assumed that the isophote axis ratio was not a function of color.

Given the somewhat eclectic nature of the F97 sample, it is prudent to check that the shapes of the F97 ellipticals are representative of elliptical galaxies as a whole, and are not biased toward nearly round or highly flattened shapes. To find an overall average shape for each elliptical, I compute the luminosity-weighted mean axis ratio \bar{q} , as detailed in Ryden (1992). The value of \bar{q} was computed within the isophote at which $\mu_V = 19.80 \text{ mag arcsec}^{-2}$, corresponding, for a galaxy with $B - V = 0.95$, to the surface brightness $\mu_B = 20.75 \text{ mag arcsec}^{-2}$ used to define the fiducial diameter D_n (Dressler et al. 1987). Defined in this manner, the mean and standard deviation of \bar{q} for the 44 ellipticals in the F97 sample are 0.796 ± 0.114 . I compute \bar{q} in the identical manner for a sample of 165 bright nearby ellipticals observed by Djorgovski (1985), 26 of which are also in the F97 compilation. The mean and standard deviation of \bar{q} for the galaxies in the Djorgovski (1985) sample are 0.803 ± 0.103 . A KS test comparing the distribution of \bar{q} for the two samples indicates that they are statistically indistinguishable, with $P_{\text{KS}} = 0.67$. Other studies in which the mean axis ratio \bar{q} is defined in different ways, yield distributions of \bar{q} which are similar to those of the F97 and Djorgovski (1985) sample: a distribution peaking at $\bar{q} \sim 0.8$, with relatively few galaxies at $\bar{q} \sim 1$ (Benacchio & Galletta 1980; Fasano & Vio 1991; Franx, Illingworth, & de Zeeuw 1991; Lambas, Maddox, & Loveday 1992). Thus, the F97 is not obviously biased toward round or flattened ellipticals.

By combining the *HST* isophotes with the ground-based isophotes, where available, I had, for each galaxy, a knowledge of the isophotal axis ratio $q \equiv b/a$ and surface brightness μ as a function of the semimajor axis a . However, from a physical point of view, it is more useful to label each isophote with its dynamical time t_{dyn} than with its value of a in arcseconds or in parsecs. The definition I use for dynamical time is (Binney & Tremaine 1987)

$$t_{\text{dyn}} = \frac{\pi}{2} \left(\frac{G[M(r) + M_{\bullet}]}{r^3} \right)^{-1/2}, \quad (1)$$

where $M(r)$ is the stellar mass within a sphere of radius r and M_{\bullet} is the mass of the central MDO (if any). The dynamical time defined in this way is 1/4 the orbital time of a star on a circular orbit with radius r .

To find the spherically averaged luminosity distribution of each galaxy, I start with the surface brightness profile $\mu(R)$, where $R \equiv q^{1/2}a$, deconvolve the surface brightness to find the luminosity density $\nu(r)$, then integrate to find the luminosity $L(r)$. The transition from the luminosity profile $L(r)$ to the mass profile $M(r)$ was made using the assumption of a constant mass-to-light ratio

Υ . For 15 of the 22 core galaxies and 5 of the 22 power law galaxies, a best-fitting value of Υ and a best-fitting value of M_{\bullet} was calculated by Magorrian et al. (1998); for these galaxies, I use the best-fitting Magorrian et al. values for Υ and M_{\bullet} . To the remaining galaxies, unfitted by Magorrian et al., I assigned a mass-to-light ratio Υ according to the relation

$$\log(\Upsilon/\Upsilon_{\odot}) = -1.11 + 0.18 \log(L_{\text{gal}}/L_{\odot}) , \quad (2)$$

which Magorrian et al. (1998) found to be the formal best-fitting straight line to $(\log L_{\text{gal}}, \log \Upsilon)$ for the early-type galaxies in their sample. There remains the problem of assigning a value of M_{\bullet} to those galaxies in my sample that were not kinematically modeled by Magorrian et al. (1998). For both power law galaxies and core galaxies Magorrian (1998) found that the parameter $x \equiv M_{\bullet}/M_{\text{gal}}$ was well fit by a Gaussian in $\log x$. For core galaxies, the mean and standard deviation in $\log x$ were $(-2.13, 0.31)$; for power law galaxies, the mean and standard deviation were $(-2.57, 0.55)$. For the purposes of computing approximate dynamical times, I assigned an MDO mass of $x = 10^{-2.13} = 0.0074$ to core galaxies not modeled by Magorrian et al. and a mass of $x = 10^{-2.57} = 0.0027$ to power law galaxies.

The approximate value of $t_{\text{dyn}}(r)$ found by the method outlined above is, of course, laden with errors. I assume spherical symmetry; this is a minor source of error. I also assume that the value of Υ found by Magorrian et al. (1998) for the central regions of galaxies can be safely used in the outer regions as well. If the mass-to-light ratio actually increases with radius, then my estimates of the dynamical time will actually be overestimates. I also ignore the observed spread in $\log x$ for each class of galaxy when assigning values of x to the ellipticals without kinematic information. The uncertainty in x leads to significant uncertainty in the dynamical time only within the radius r_{eq} at which $M(r) = M_{\bullet}$. For the 5 power law ellipticals fitted by Magorrian et al. (1998) the median value of r_{eq} was only 8 pc, with a corresponding dynamical time of $t_{\text{eq}} \approx 0.04$ Mpc. For the 15 core galaxies fitted, the median value of r_{eq} was 230 pc, with a corresponding dynamical time of $t_{\text{eq}} \approx 0.9$ Mpc. The standard deviation in $\log x$ of 0.31 for core galaxies corresponds to an uncertainty of a factor 2 in M_{\bullet} . In the region where $r \ll r_{\text{eq}} \approx 230$ pc, this leads to a 43% uncertainty in t_{dyn} for a given value of r , or equivalently, a 27% uncertainty in r for a fixed value of t_{dyn} .

One last cautionary note about MDO masses: the values of M_{\bullet} deduced by Magorrian et al. (1998) are dependent on the two-integral models which they assume for the kinematics. If the velocity dispersion is allowed to be radially anisotropic, then the central MDO mass required will be reduced. The limited information available about velocity anisotropy in the centers of ellipticals, as reviewed by van der Marel (1998), is consistent with core galaxies being radially anisotropic and power law galaxies being roughly isotropic, but the uncertainties are still great. If, in fact, the Magorrian et al. (1998) masses are overestimates, then the values of t_{dyn} computed in this paper will be too short within the region inside r_{eq} . Outside r_{eq} , the dynamical times are not greatly affected by the MDO mass assumed.

For each galaxy in my sample, I compute t_{dyn} as a function of semimajor axis, in the range

$0.1'' < a < a_{\max}$, where a_{\max} is the semimajor axis of the outermost isophote in the ground-based photometry. The minimum value of $a = 0.1''$ corresponds to the resolution limit of the *HST* Planetary Camera images. For the 22 core galaxies in the sample, the median dynamical time at $a = 0.1''$ is 0.03 Myr; for the 22 power law galaxies, the median dynamical time at $a = 0.1''$ is 0.08 Myr. For the 22 core galaxies, the median dynamical time at $a = a_{\max}$ is 150 Myr; for the 22 power law galaxies, the median dynamical time at $a = a_{\max}$ is 60 Myr. Thus, when making statistical comparisons between the core galaxies and power law galaxies, the statistics are best in the range $0.08 \text{ Myr} \lesssim t_{\text{dyn}} \lesssim 60 \text{ Myr}$. (The more restricted range of dynamical times for which *all* galaxies in the sample have isophotal data is $0.3 \text{ Myr} < t_{\text{dyn}} < 8 \text{ Myr}$.)

3. Analysis

Once each isophote has a dynamical time t_{dyn} and apparent axis ratio q associated with it, I can examine the distribution of q at fixed values of t_{dyn} for selected subsamples of ellipticals. As a first step in the analysis, Figure 1 shows the mean value of q (upper lines) and the standard deviation of q (lower lines) as a function of dynamical time. The solid lines indicate the mean and standard deviation for the core galaxies; the dashed lines are the values for the power law galaxies. For a wide range of dynamical times, $0.1 \text{ Myr} \lesssim t_{\text{dyn}} \lesssim 50 \text{ Myr}$, the core galaxies are rounder on average than the power law galaxies, and have a narrower distribution of q . Moreover, though there is no systematic trend in the average value of q with t_{dyn} for the power law galaxies, the core galaxies become steadily flatter on average for $t_{\text{dyn}} \gtrsim 2 \text{ Myr}$ and for $t_{\text{dyn}} \lesssim 0.2 \text{ Myr}$.

Are the differences in projected shape between core galaxies and power law galaxies statistically significant? After all, there are at most 22 galaxies of each type at a given t_{dyn} , and 22 is not a huge number. To test whether the shapes of core galaxies and power law galaxies are drawn from the same parent distribution, I performed KS tests. The results of the comparison between the distribution of q for core galaxies and for power law galaxies is shown in Figure 2. The KS probability is $P_{\text{KS}} < 0.01$ only in the limited range $0.48 \text{ Myr} < t_{\text{dyn}} < 3.3 \text{ Myr}$; within this range, the shapes of the core galaxies in my sample are different, at the 99% confidence level, from those of the power law galaxies. Both in the central regions of galaxies, where $t_{\text{dyn}} \lesssim 0.2 \text{ Myr}$, and in the outer regions, where $t_{\text{dyn}} \gtrsim 20 \text{ Myr}$, the shape distribution for core galaxies is statistically indistinguishable, at the 90% confidence level, from that of power law galaxies.

The puzzling question is why the intermediate region of core ellipticals, where $t_{\text{dyn}} \sim 1 \text{ Myr}$, should be rounder on average than both the central region, where $t_{\text{dyn}} \lesssim 0.2 \text{ Myr}$, and the outer region, where $t_{\text{dyn}} \gtrsim 20 \text{ Myr}$. The shape of the central regions is unfortunately complicated, in many cases, by the presence of substructure. Among the 44 ellipticals I am examining, the radius at which $t_{\text{dyn}} = 0.2 \text{ Myr}$ ranges from about 8 parsecs for the low luminosity elliptical VCC 1199 to 150 parsecs for the brightest cluster galaxy NGC 6166, with a typical value of a few tens of parsecs. This is the length scale on which elliptical galaxies frequently display signs of having stellar disks (van den Bosch et al. 1994, Faber et al. 1997), dust disks and rings (van Dokkum

& Franx 1995), stellar nuclei (Lauer et al. 1995), and kinematically distinct cores. Due to the relative complexity of the central regions of ellipticals, I will not analyze in detail their shapes in this paper, concentrating on the intermediate ($t_{\text{dyn}} \sim 1$ Myr) and outer ($t_{\text{dyn}} \gtrsim 20$ Myr) regions.

Although the mean and standard deviation of q , as plotted in Figure 1, are valuable bits of information, they don’t provide all the information contained in $f(q)$, the full distribution of apparent shapes at a given t_{dyn} . Since a full knowledge of $f(q)$ provides important constraints on the permissible range of intrinsic shapes, I will examine in detail the distribution of q for isophotes at two selected dynamical times. The inner isophote will lie in the regime $0.48 \text{ Myr} < t_{\text{dyn}} < 3.3 \text{ Myr}$, where the shapes of the core and power law ellipticals are significantly different, and the outer isophote in the regime $t_{\text{dyn}} > 20 \text{ Myr}$, where their shapes are statistically indistinguishable.

For the shorter dynamical time, and inner isophote, I choose $t_{\text{dyn}} = 0.75$ Myr. The axis ratio q_{in} is then defined as the observed axis ratio of the isophote with semimajor axis $a = r_{\text{in}}$, where $t_{\text{dyn}}(r_{\text{in}}) = 0.75$ Myr. In angular units, the values of r_{in} for the sample range from 0.16 arcsec for Abell 1020 to 14 arcsec for the nearby compact elliptical NGC 221. In physical units, the values of r_{in} range from 32 pc for VCC 1440 to 330 pc for NGC 6166.

For core ellipticals, a uniquely interesting length scale is the break radius at which the slope of the surface brightness profile changes. Faber et al. (1997) computed a break radius r_b by fitting a “nuker” law (Lauer et al. 1995),

$$\mu(r) = 2^{(\beta-\gamma)/\alpha} \mu_b \left(\frac{r}{r_b}\right)^\gamma \left[1 + \left(\frac{r}{r_b}\right)^\alpha\right]^{(\gamma-\beta)/\alpha}. \quad (3)$$

The dynamical time at the break radius varies from one core galaxy to another; for the core ellipticals in the F97 sample, the value of $t_{\text{dyn}}(r_b)$ ranges from 0.03 Myr for NGC 4486B to 4.6 Myr for NGC 6166, with a median value of 0.9 Myr. For most of the core ellipticals in the sample, r_{in} , as defined above, is comparable to r_b ; the values of r_{in} range from $0.24r_b$ for NGC 1600 to $9.6r_b$ for NGC 4486B, with a median value of $r_{\text{in}} = 0.7r_b$.

For the longer dynamical time, and outer isophote, I choose $t_{\text{dyn}} = 50$ Myr. The axis ratio q_{out} is then defined as the observed axis ratio of the isophote with $a = r_{\text{out}}$, where $t_{\text{dyn}}(r_{\text{out}}) = 50$ Myr. For 2 of the core galaxies and 7 of the power law galaxies in the sample, r_{out} lies outside the region where published surface photometry is available. For the galaxies in the sample with photometry available out to r_{out} , the angular size of r_{out} ranges from 8.7 arcsec for Abell 1831 to 210 arcsec for NGC 4472. In physical units, the values of r_{out} range from 3.2 kpc for NGC 4458 to 16 kpc for NGC 1600. For the core galaxies, r_{out} always lies well outside the break radius; the values of r_{out} range from $10r_b$ for NGC 4874 to $230r_b$ for NGC 3608.

Values of q_{in} and q_{out} for the core galaxies in the sample are given in Table 1; values of q_{in} and q_{out} for the power law galaxies are given in Table 2. The cumulative distribution functions are displayed graphically in Figure 3. The upper panel shows the distribution of q_{in} and q_{out} for the core galaxies; the lower panel shows the equivalent distributions for the power law galaxies. In each

panel, the solid line gives the distribution of q_{in} , and the dotted line gives the distribution of q_{out} . A glance at Figure 3 shows that q_{in} for the core galaxies has a significantly different distribution from the other three populations. This visual impression is confirmed by a Kolmogorov-Smirnov test applied to the different distributions. The results of the KS test are displayed in Table 3. The only pairs of distributions which differ at the 99% confidence level, as measured by the KS test, are q_{in} for core galaxies and q_{out} for core galaxies, with $P_{\text{KS}} = 0.0059$, and q_{in} for core galaxies and q_{in} for power law galaxies, with $P_{\text{KS}} = 0.0029$.

Within the subsample of core ellipticals, q_{in} is uncorrelated with the absolute magnitude M_V of the galaxy; a similar lack of correlation between q_{in} and M_V is seen within the subsample of power law ellipticals. This indicates that the difference in q_{in} between core and power law ellipticals is not simply a luminosity-dependent effect, reflecting the greater average luminosity of core galaxies, but rather is more fundamentally linked to the physical difference between core and power law galaxies. (This result also suggests that the finding of Tremblay & Merritt [1996] – that bright ellipticals ($M_B < -20$) are rounder than faint ellipticals – is based on the fact that core ellipticals are rounder than power law ellipticals in their inner regions. The luminosity-weighted mean axis ratio used by Tremblay & Merritt is strongly weighted to the bright inner regions of the galaxies, where the core ellipticals, which dominate the $M_B < -20$ sample, are rounder than power law ellipticals.)

Instead of looking at the cumulative distribution function, $F(q)$, for a sample of N axis ratios, I can compute a nonparametric kernel estimate of the distribution function $f(q)$, defined so that $f(q)dq$ is the fraction of all galaxies with axis ratios in the range $q \rightarrow q + dq$. A full discussion of using nonparametric estimates for $f(q)$ is given by Tremblay & Merritt (1995) and Ryden (1996); I will give only a brief outline here. Given a sample q_1, q_2, \dots, q_N of apparent axis ratios, the kernel estimate of $f(q)$ is

$$\hat{f}(q) = \frac{1}{Nh} \sum_{i=1}^N K\left(\frac{q - q_i}{h}\right), \quad (4)$$

where K is the kernel function. To produce a smooth differentiable estimate, I used a Gaussian function,

$$K(x) = \frac{1}{\sqrt{2\pi}} e^{-x^2/2}, \quad (5)$$

of width $h = 0.9\sigma N^{-0.2}$, where σ is the standard deviation of the sample. This kernel width, for distributions that are not strongly skewed, minimizes the integrated mean square error (Vio et al. 1994). Because q is limited to the range $0 \leq q \leq 1$, I use reflective boundary conditions at $q = 0$ and $q = 1$ to ensure the proper normalization for $\hat{f}(q)$. Because these boundary conditions are artificially imposed, the prudent reader will not place much confidence in the shape of \hat{f} within a distance $\sim h$ of the boundaries at $q = 0$ and $q = 1$.

Error intervals can be placed on the estimated \hat{f} by a process of bootstrap resampling (Merritt & Tremblay 1994). From the original data set q_1, q_2, \dots, q_N , I draw, with replacement, a new set of N data points and compute a new estimate of \hat{f} . After making 1000 bootstrap estimates,

I use them to place error intervals on the original estimate \hat{f} . For instance, the 80% confidence interval at a given value of q is the range in \hat{f} such that 10% of the bootstrap estimates lie above the interval and 10% of the bootstrap estimates lie below the interval.

The upper panel of Figure 4 shows the distribution of apparent shapes for the inner isophotes of core galaxies, where $t_{\text{dyn}} = 0.75$ Myr. The solid line is the best estimate for $\hat{f}(q_{\text{in}})$; the dashed lines give the 80% error interval and the dotted lines give the 98% error interval. The peak in \hat{f} is at $q_{\text{in}} = 0.91$ (a nearly round shape, equivalent to an E1 galaxy). The corresponding distribution for the shapes of the outer isophotes of core galaxies is given in the upper panel of Figure 5; note that the peak in \hat{f} for the outer regions is at $q_{\text{out}} = 0.76$. The distribution of apparent shapes for the inner regions of power law galaxies is shown in the upper panel of Figure 6. The corresponding distribution of shapes for the outer regions of power law galaxies is shown in the upper panel of Figure 7. Note that the distribution \hat{f} peaks at $q_{\text{in}} \approx 0.7$ for power law galaxies, in both their inner and outer regions.

So far, I have dealt only with the apparent projected shapes of galaxies, and not with their intrinsic three-dimensional shapes. For an individual galaxy, it is impossible to determine the intrinsic shape merely from a knowledge of the projected photometry. However, if I assume that the galaxies in a sample are all randomly oriented oblate spheroids, I can perform a mathematical inversion of $\hat{f}(q)$ to find the underlying distribution $\hat{f}_o(\gamma)$ of intrinsic shapes, where $\gamma = c/a$ is the intrinsic axis ratio of the oblate spheroid, with $0 \leq \gamma \leq 1$. Similarly, if I assume that the galaxies are randomly oriented *prolate* spheroids, I can perform an inversion to find $\hat{f}_p(\gamma)$, the underlying distribution of axis ratios for the prolate galaxies.

The game of finding the distribution of intrinsic shapes of elliptical galaxies, using the oblate and prolate hypotheses, has been played for several decades (Hubble 1926; Sandage et al. 1970; Binney & de Vaucouleurs 1981). The use of kernel estimates and bootstrap resampling permits us to reject or accept the oblate hypothesis (or the prolate hypothesis) at a given level of statistical confidence. For instance, I can take a given sample of axis ratios, and invert the best estimate \hat{f} and the estimate for each of the 1000 bootstrap resamplings, using the hypothesis that the galaxies are randomly oriented oblate spheroids. This gives me a best estimate for $\hat{f}_o(\gamma)$ as well as 1000 bootstrap estimates. At each value of γ , an upper limit can be placed on \hat{f}_o at the 90% confidence level, for example, by finding the value of \hat{f}_o such that 10% of the bootstrap estimates fall above this value. If this upper confidence level falls below zero, then the oblate hypothesis can be rejected at the 90% (one-sided) confidence level, since negative values of \hat{f}_o are unphysical. Similar analysis of \hat{f}_p can be used to reject or accept the prolate hypothesis.

For the inner regions of core galaxies, where $t_{\text{dyn}} = 0.75$ Myr, the nonparametric estimate \hat{f}_o , given the oblate hypothesis, is shown in the middle panel of Figure 4. The best fit (shown as the solid line) dips below zero for γ close to one, but given the width of the error intervals, the oblate hypothesis cannot be rejected at the 90% confidence level. The best fitting \hat{f}_o peaks at $\gamma = 0.86$, with a hint of a secondary peak at $\gamma = 0.68$. The prolate hypothesis, illustrated in the

bottom panel of Figure 4, is statistically acceptable for the inner region of core galaxies; \hat{f}_p peaks at $\gamma = 0.87$.

For the outer regions of core galaxies, where $t_{\text{dyn}} = 50$ Myr, the best estimate for \hat{f}_o is shown in the middle panel of Figure 5. The best fit, shown as the solid line, dips below zero for $\gamma > 0.83$, and the upper bound of the 98% confidence interval is below zero for $\gamma > 0.932$. Thus, the oblate hypothesis can be rejected at the 99% one-sided confidence level. The prolate hypothesis, as indicated by the bottom panel of Figure 5, can also be rejected at the 99% confidence level. Thus, at least some amount of triaxiality must be present to explain the observed lack of nearly circular isophotes.

Once the hypothesis of axisymmetry is abandoned, it requires two axis ratios, $\beta = b/a$ and $\gamma = c/a$, to describe the shape of a triaxial galaxy. For a population of triaxial systems, the distribution of intrinsic axis ratios, $f_t(\beta, \gamma)$, is no longer uniquely determined by the distribution of observed axis ratios, $f(q)$. However, I can determine a permissible distribution of intrinsic axis ratios by assuming a parametric form for f_t and adjusting the parameters to yield the best fit. For instance, assume that the outer regions of the core galaxies in my sample have intrinsic axis ratios distributed according to the law

$$f_t(\beta, \gamma) \propto \exp \left[-\frac{(\beta - \beta_0)^2 + (\gamma - \gamma_0)^2}{2\sigma_0^2} \right]. \quad (6)$$

(There is no particular physical reason to expect f_t to be an isotropic Gaussian in (β, γ) space; this is merely a convenient parameterization.) The best-fitting set of parameters, as measured by a KS test to the observed axis ratios of the outer regions of core galaxies, is $\beta_0 = 0.72$, $\gamma_0 = 0.71$, and $\sigma_0 = 0.037$, with a KS probability of $P_{\text{KS}} = 0.997$. Although the peak of this distribution is at a nearly prolate shape, it is also possible to get a good fit with a model in which the most probable shape is oblate ($\beta_0 = 1$, $\gamma_0 = 0.67$, and $\sigma_0 = 0.056$, yielding $P_{\text{KS}} = 0.87$).

For the inner regions of power law galaxies, where $t_{\text{dyn}} = 0.75$ Myr, the nonparametric estimate for \hat{f}_o is shown in the middle panel of Figure 6. Although the best fit to \hat{f}_o , given by the solid line, drops below zero for $\gamma > 0.75$, the oblate hypothesis, given the width of the error intervals, can't be ruled out at the 91% confidence level. The best fit to \hat{f}_o peaks at $\gamma = 0.64$; if the inner regions of power law galaxies are randomly oriented oblate objects, then very few of them can be rounder than $\gamma \approx 0.8$. The prolate hypothesis, as shown in the bottom panel of Figure 6, is statistically acceptable; it also leads to the conclusion that few power law galaxies have inner regions rounder than $\gamma \approx 0.8$.

Since the outer and inner regions of power law galaxies have a similar distribution of apparent shapes, the nonparametric estimate of \hat{f}_o for the outer regions of power law ellipticals, shown as the middle panel of Figure 7, is similar to that for the inner regions, shown as the middle panel of Figure 6. For the outer regions, the best fit peaks at $\gamma = 0.65$, with few galaxies, under the oblate hypothesis, being rounder than $\gamma \approx 0.8$. The prolate hypothesis, illustrated in the bottom panel of Figure 7, is also statistically acceptable for power law galaxies.

The distributions of q_{out} for the core galaxies and the power law galaxies in my sample are statistically indistinguishable ($P_{\text{KS}} = 0.55$). Thus, it is illuminating to adopt the hypothesis that the shapes of elliptical galaxies in the regime for $t_{\text{dyn}} \approx 50$ Myr is independent of whether their central density cusps are steep or shallow. With this hypothesis, the samples of q_{out} for core galaxies and power law galaxies can be combined, to provide better statistics. The combined sample has 34 galaxies (20 core, 14 power law). For the combined sample, $\hat{f}(q_{\text{out}})$ peaks at $q_{\text{out}} = 0.75$. The lack of nearly circular galaxies in the combined sample, along with the narrower error intervals, means that both the oblate hypothesis and the prolate hypothesis can be rejected at the 99% confidence level. However, the distribution of q_{out} for the combined sample of core and power law galaxies can be well fit by a population of triaxial shapes. The best-fitting parametric function $f_t(\beta, \gamma)$ of the form given in equation (6) has parameters $\beta_0 = 0.73$, $\gamma_0 = 0.70$, and $\sigma_0 = 0.095$, yielding $P_{\text{KS}} = 0.97$. However, acceptable fits are also provided by models in which the most probable shape is oblate ($\beta_0 = 1$, $\gamma_0 = 0.64$, and $\sigma_0 = 0.086$, yielding $P_{\text{KS}} = 0.78$) and by models in which the most probable shape is prolate ($\beta_0 = \gamma_0 = 0.71$ and $\sigma_0 = 0.073$, yielding $P_{\text{KS}} = 0.95$).

4. Summary and Discussion

In their outer regions, where $t_{\text{dyn}} \gtrsim 20$ Myr, the core ellipticals in the F97 sample have a distribution of apparent shapes which is indistinguishable from that of the power law ellipticals. The scarcity of elliptical galaxies with circular isophotes in their outer regions implies that they are probably not all oblate or prolate objects. Due to the degeneracy of the problem, it cannot be determined, from the surface photometry alone, whether the majority of elliptical galaxies are nearly oblate, nearly prolate, or highly triaxial in their outer regions. (Moreover, even if core ellipticals and power law ellipticals have an identical distribution of apparent shapes in projection, this does not demand, although it does permit, an identical distribution of intrinsic shapes.)

The most intriguing result of my analysis is that in the region where $0.5 \text{ Myr} \lesssim t_{\text{dyn}} \lesssim 3 \text{ Myr}$, the core ellipticals are significantly rounder than the power law ellipticals. In this regime, the oblate hypothesis is acceptable for core ellipticals, with a distribution of intrinsic axis ratios peaking at a fairly round shape, $\gamma \approx 0.86$. In the very central regions, $t_{\text{dyn}} \ll 0.5 \text{ Myr}$, the core ellipticals become flatter again on average, probably due, in part, to the presence of circumnuclear stellar disks seen in projection.

How can we explain the observation that core galaxies are so nearly spherical in the region where $0.5 \text{ Myr} \lesssim t_{\text{dyn}} \lesssim 3 \text{ Myr}$? This region is far enough from the center that circumnuclear disks of stars, gas, and dust don't strongly affect the isophote shape, but has orbital times short enough for a central MDO to have completed chaotic mixing. The observed shapes of core galaxies are consistent with their being nearly spherical and nearly oblate in their inner regions, and more flattened and more triaxial in their outer regions, just as we would naively expect from the effects of a central MDO. The shape transition occurs at dynamical times of ~ 5 Myr, or orbital times of

~ 20 Myr. The observation that power law galaxies have the same distribution of apparent shapes in their inner and outer regions seems to indicate that the central density cusp and MDO in power law galaxies is not effective at driving the stellar orbits in the central region to more spherical stochastic shapes.

The observed difference in shape between core ellipticals and power law ellipticals may be linked to a difference in their origins. Faber et al. (1997) have proposed a scenario in which cores with shallow cusps are the result of the orbital decay of MDOs accreted during galaxy mergers. Numerical simulations of the evolution of binary black holes in the centers of galaxies (Quinlan & Hernquist 1997) has shown that the galaxy’s stellar distribution develops a central core as stars are ejected from the central cusp by the black hole binary. The mass of the stellar core which develops is roughly 5 times the mass of the black hole binary. For the core ellipticals kinematically modeled by Magorrian et al. (1998), the radius r_c at which $M(r_c) \approx 5M_\bullet$ ranges from 90 to 7000 parsecs, with a median value of 600 parsecs. The dynamical time at r_c in these core galaxies ranges from 0.5 to 26 million years, with a median value of 2.3 Myr. These dynamical times are intriguingly close to the dynamical time ~ 5 Myr at which core ellipticals make the transition from being flattened and triaxial to being more nearly spherical.

This work was supported by NSF grant AST 93-57396. Marcella Carollo, Tod Lauer, and Frank van den Bosch provided me with isophotal data. Rick Pogge, David Merritt, and an anonymous referee made useful comments.

REFERENCES

- Barnes, J. E. 1992, *ApJ*, 393, 484
- Benacchio, L., & Galletta, G. 1980, *MNRAS*, 193, 885
- Binney, J., & de Vaucouleurs, G. 1981, *MNRAS*, 194, 679
- Bower, G., et al. 1998, *ApJ*, 492, L111
- Caon, N., Capaccioli, M., & D’Onofrio, M. 1994, *A&AS*, 106, 199 (C94)
- Caon, N., Capaccioli, M., & Rampazzo, R. 1990, *A&AS*, 86, 429 (C90)
- Capaccioli, M., Piotto, G., & Rampazzo, R. 1988, *AJ*, 96, 487 (C88)
- Carollo, C. M., Franx, M., Illingworth, G. D., & Forbes, D. A. 1997, *ApJ*, 481, 710
- de Vaucouleurs, G., de Vaucouleurs, A., & Corwin, H. G. 1976, *Second Reference Catalog of Bright Galaxies* (U. of Texas Press, Austin)
- de Zeeuw, T. 1985, *MNRAS*, 216, 273
- Djorgovski, S. 1985, Ph.D. thesis, Univ. California, Berkeley
- Dressler, A., Lynden-Bell, D., Burstein, D., Davies, R. L., Faber, S. M., Terlevich, R., & Wegner, G. 1987, *ApJ*, 313, 42
- Faber, S. M., et al. 1997, *AJ*, 114, 1771
- Fasano, G., & Vio, R. 1991, *MNRAS*, 249, 629
- Ferrarese, L., Ford, H. C., & Jaffe, W. 1996, *ApJ*, 470, 444
- Franx, M., Illingworth, G. D., & de Zeeuw, P. T. 1991, *ApJ*, 383, 112
- Fridman, T., & Merritt, D. 1997, *AJ*, 114, 1479
- Gebhardt, K., et al. 1996, *AJ*, 112, 105
- Gerhard, O. E., & Binney, J. 1985, *MNRAS*, 216, 467
- Goudfrooij, P., Hansen, L., Jorgensen, H. E., Norgaard-Nielsen, H. U., de Jong, T., & van den Hoek, L. B. 1994, *A&AS*, 104, 179 (G94)
- Grillmair, C. J., Faber, S. M., Lauer, T. R., Baum, W. A., Lynds, C. R., O’Neil, E. J., & Shaya, E. J. 1994, *AJ*, 108, 102
- Harms, R. J., et al. 1994, *ApJ*, 435, L35

- Hubble, E. P. 1926, *ApJ*, 64, 321
- Jaffe, W., Ford, H. C., O’Connell, R. W., van den Bosch, F. C., & Ferrarese, L. 1994, *AJ*, 108, 1567
- Kormendy, J., & Richstone, D. 1995, *ARA&A*, 33, 581
- Kuijken, K. 1993, *ApJ*, 409, 68
- Kuzmin, G. G. 1956, *Astr. Zh.*, 33, 27
- Lambas, D. G., Maddox, S., & Loveday, J. 1992, *MNRAS*, 258, 404
- Lauer, T. R. 1985, *ApJS*, 57, 473 (L85)
- Lauer, T. R., et al. 1999, in preparation (L99)
- Lauer, T. R., Faber, S. M., Ajhar, E. A., Grillmair, C. J., & Scowen, P. A. 1998, *ApJ*, submitted (astro-ph/9806277) (L98)
- Lauer, T. R., et al. 1992, *AJ*, 103, 703 (L92)
- Lauer, T. R., et al. 1995, *AJ*, 110, 2622 (L95)
- Magorrian, J. 1998, private communication
- Magorrian, J., et al. 1998, *AJ*, 115, 2285
- Merritt, D. 1997, *ApJ*, 486, 102
- Merritt, D., & Fridman, T. 1996, *ApJ*, 460, 136
- Merritt, D., & Quinlan, G. D. 1998, *ApJ*, 498, 625
- Merritt, D., & Tremblay, B. 1994, *AJ*, 108, 514
- Norman, C. A., May, A., & van Albada, T. S. 1985, *ApJ*, 296, 20
- Peletier, R. F. 1993, *A&A*, 271, 51 (P93)
- Peletier, R. F., Davies, R. L., Illingworth, G. D., Davis, L. E., & Cawson, M. 1990, *AJ*, 100, 1091 (P90)
- Quinlan, G. D., & Hernquist, L. 1997, *New Astronomy*, 2, 533
- Reid, N., Boisson, C., & Sansom, A. E. 1994, *MNRAS*, 269, 713 (R94)
- Ryden, B. S. 1992, *ApJ*, 396, 445
- Ryden, B. S. 1996, *ApJ*, 461, 146

- Sandage, A., Freeman, K. C., & Stokes, N. R. 1970, *ApJ*, 160, 831
- Schwarzschild, M. 1993, *ApJ*, 409, 563
- Syer, D., & Zhao, H. 1998, *MNRAS*, 296, 407
- Tremblay, B., & Merritt, D. 1995, *AJ*, 110, 1039
- Tremblay, B., & Merritt, D. 1996, *AJ*, 111, 2243
- Valluri, M., & Merritt, D. 1998, *ApJ*, 506, 686
- van den Bosch, F. C., Ferrarese, L., Jaffe, W., Ford, H. C., & O’Connell, R. W. 1994, *AJ*, 108, 1579 (V94)
- van der Marel, R. P. 1998, in *Galaxy Interactions at Low and High Redshift*, IAU Symposium 186, ed. D. B. Sanders & J. Barnes (Kluwer: Dordrecht)
- van Dokkum, P. G., & Franx, M. 1995, *AJ*, 110, 2027
- Vio, R., Fasano, G., Lazzarin, M., & Lessi, O. 1994, *A&A*, 289, 640

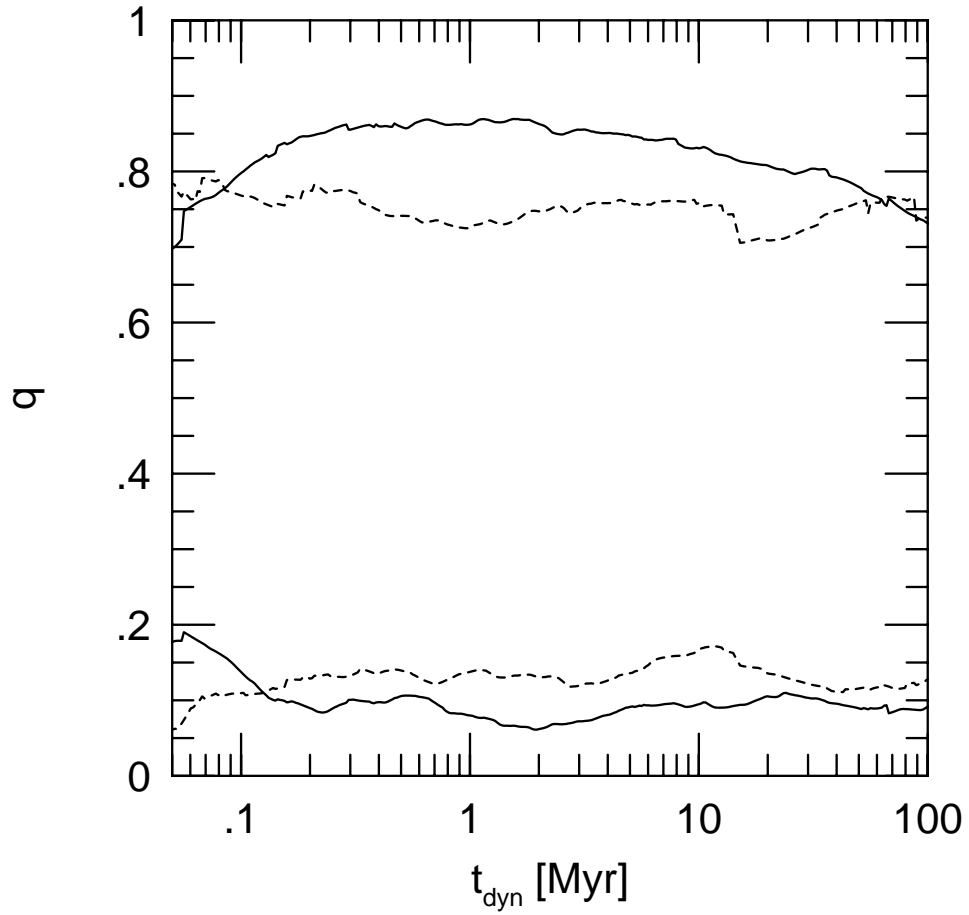


Fig. 1.— The mean (upper lines) and standard deviation (lower lines) of the axis ratio q as a function of dynamical time, for each subsample of elliptical galaxies. The solid line indicates the subsample of core ellipticals, and the dashed line indicates the subsample of power law ellipticals.

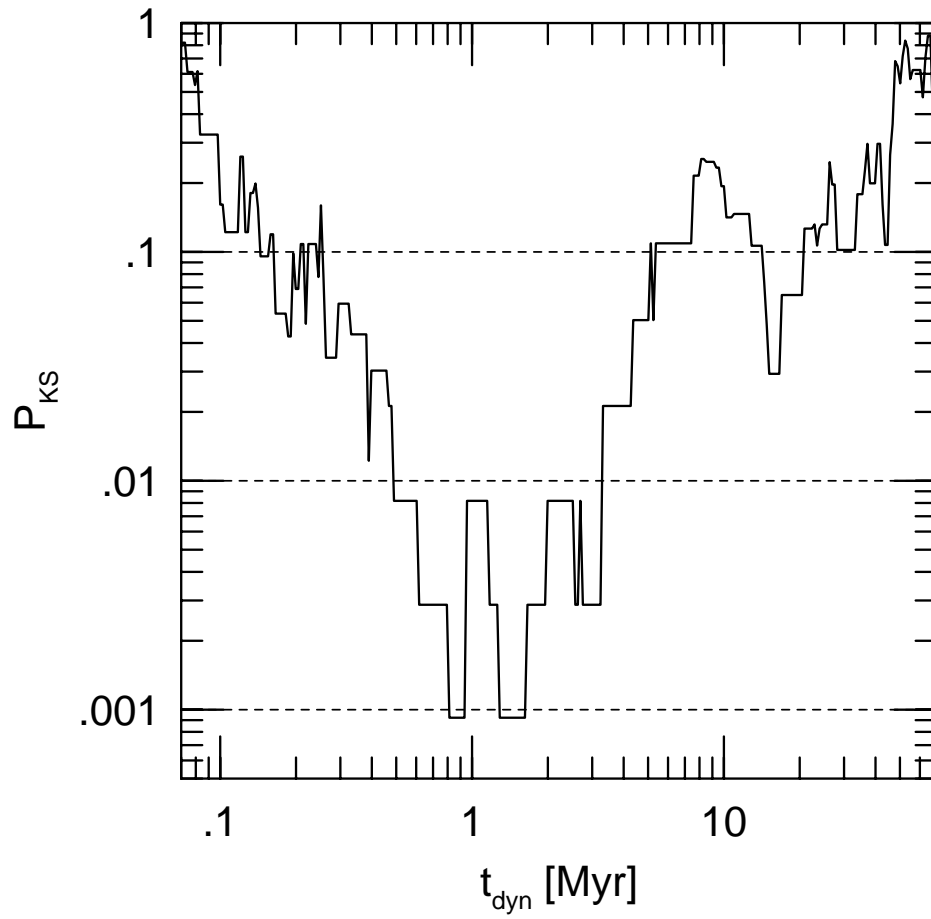


Fig. 2.— The probability yielded by a Kolmogorov-Smirnov test comparing the distribution of q for the core ellipticals with the distribution of q for the power law ellipticals.

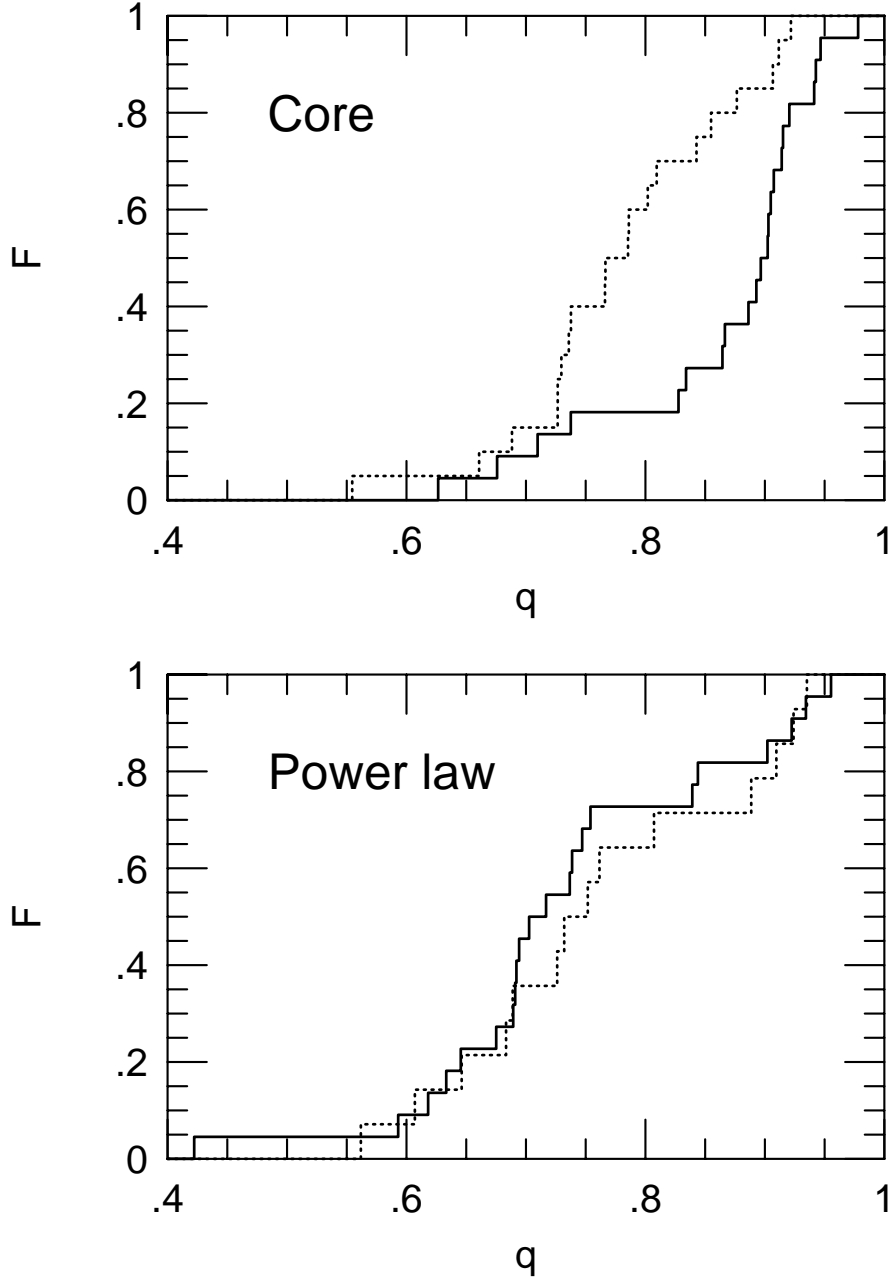


Fig. 3.— *Top*, the cumulative distribution function for the apparent axis ratios of the core galaxies in the sample. *Bottom*, the cumulative distribution function for the apparent axis ratios of the power law galaxies. In each panel, the solid line indicates the axis ratios of the $t_{\text{dyn}} = 0.75$ Myr isophote and the dotted line indicates the axis ratios of the $t_{\text{dyn}} = 50$ Myr isophote.

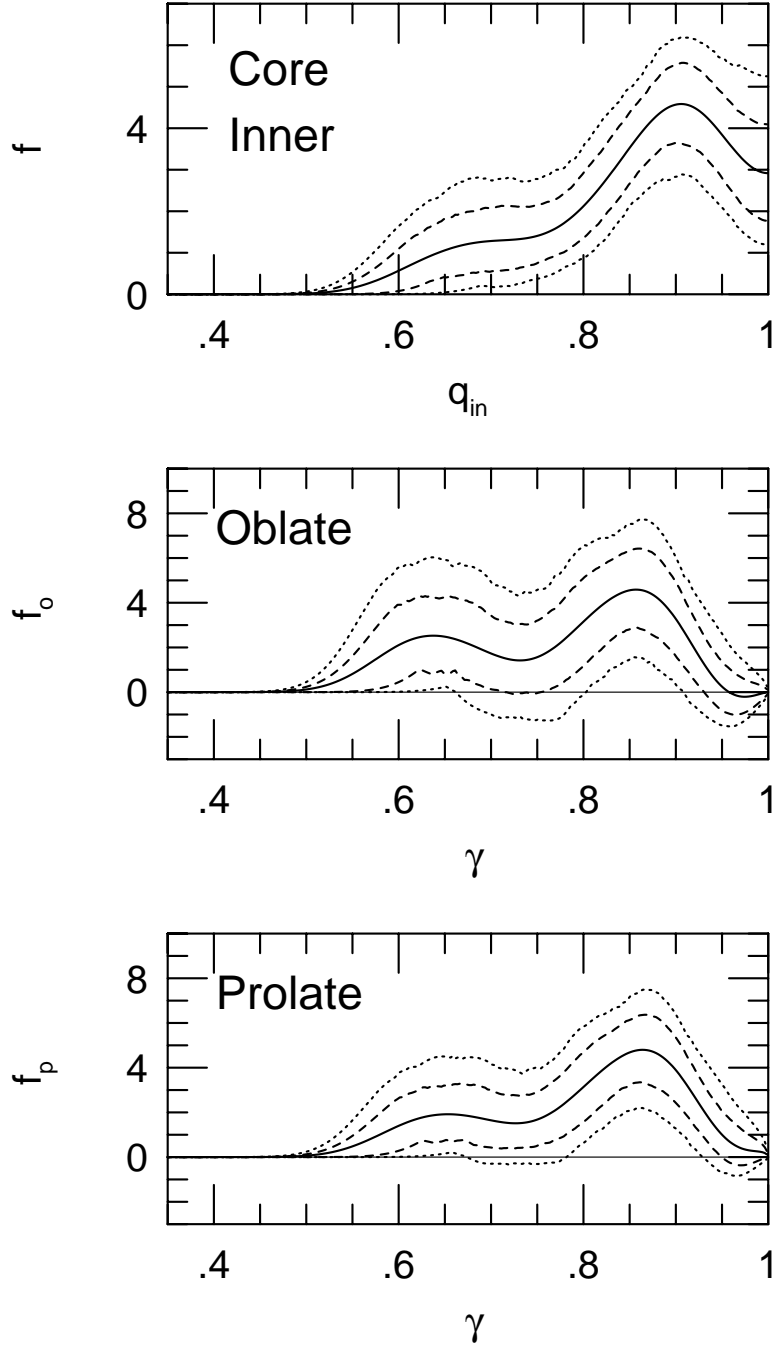


Fig. 4.— *Top*, the nonparametric kernel estimate of the distribution function of axis ratios of the $t_{\text{dyn}} = 0.75$ Myr isophotes of the core ellipticals. *Middle*, distribution of intrinsic axis ratios, assuming the intrinsic shape is oblate. *Bottom*, distribution of intrinsic axis ratios, assuming the intrinsic shape is prolate. The solid line in each panel is the best estimate, the dashed lines are the 80% confidence band, found by bootstrap resampling, and the dotted lines are the 98% confidence band. The sample contains $N = 22$ galaxies; the kernel width is $h = 0.044$.

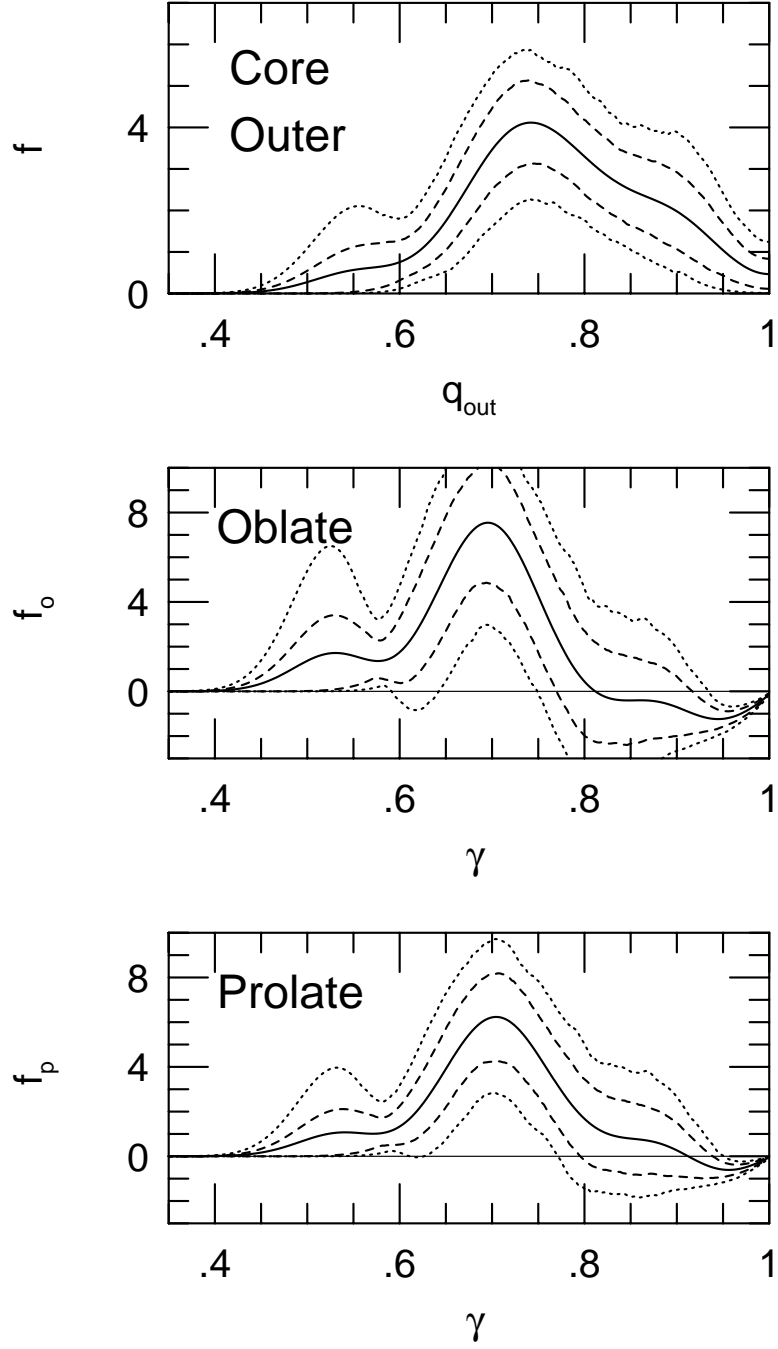


Fig. 5.— As Fig. 2, but for the $t_{\text{dyn}} = 50$ Myr isophotes of the core galaxies. The sample contains $N = 20$ galaxies; the kernel width is $h = 0.044$.

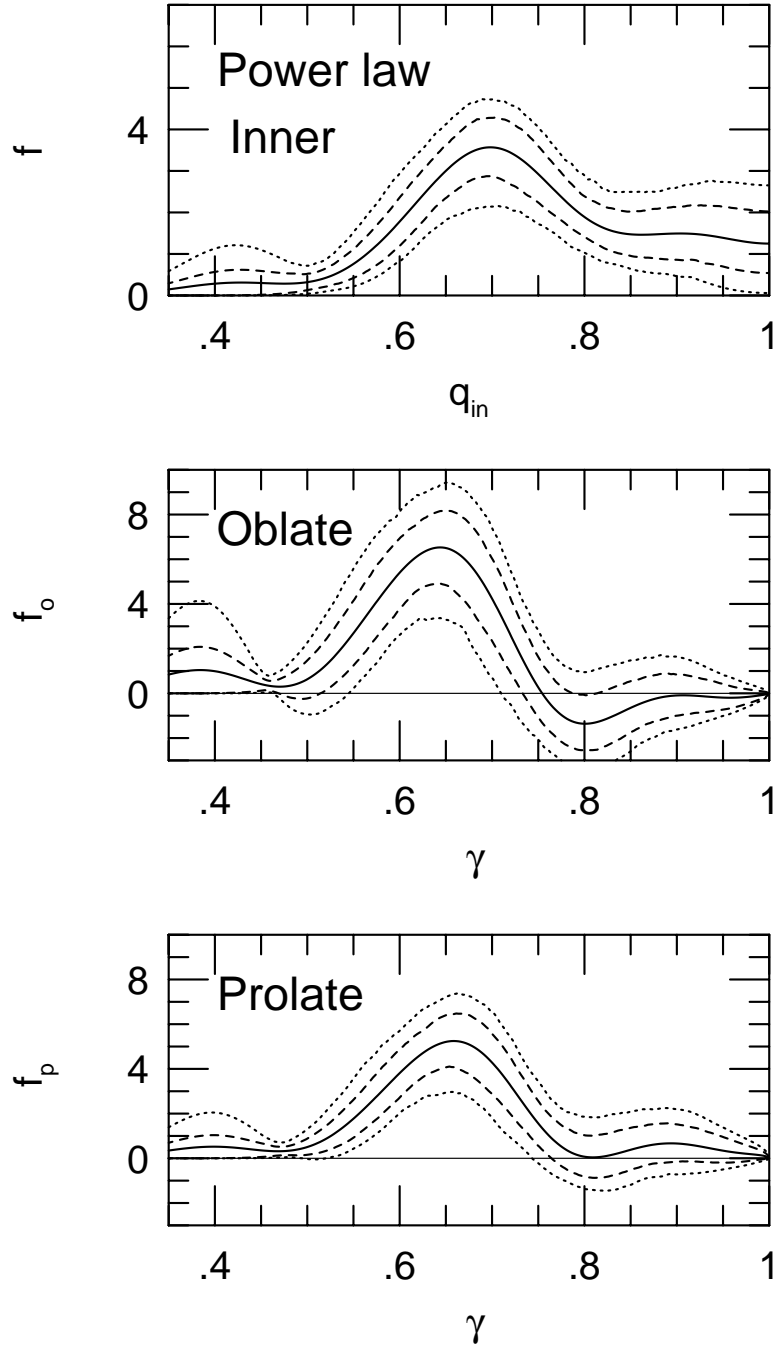


Fig. 6.— As Fig. 2, but for the $t_{\text{dyn}} = 0.75$ Myr isophotes of the power law galaxies. The sample contains $N = 22$ galaxies; the kernel width is $h = 0.060$.

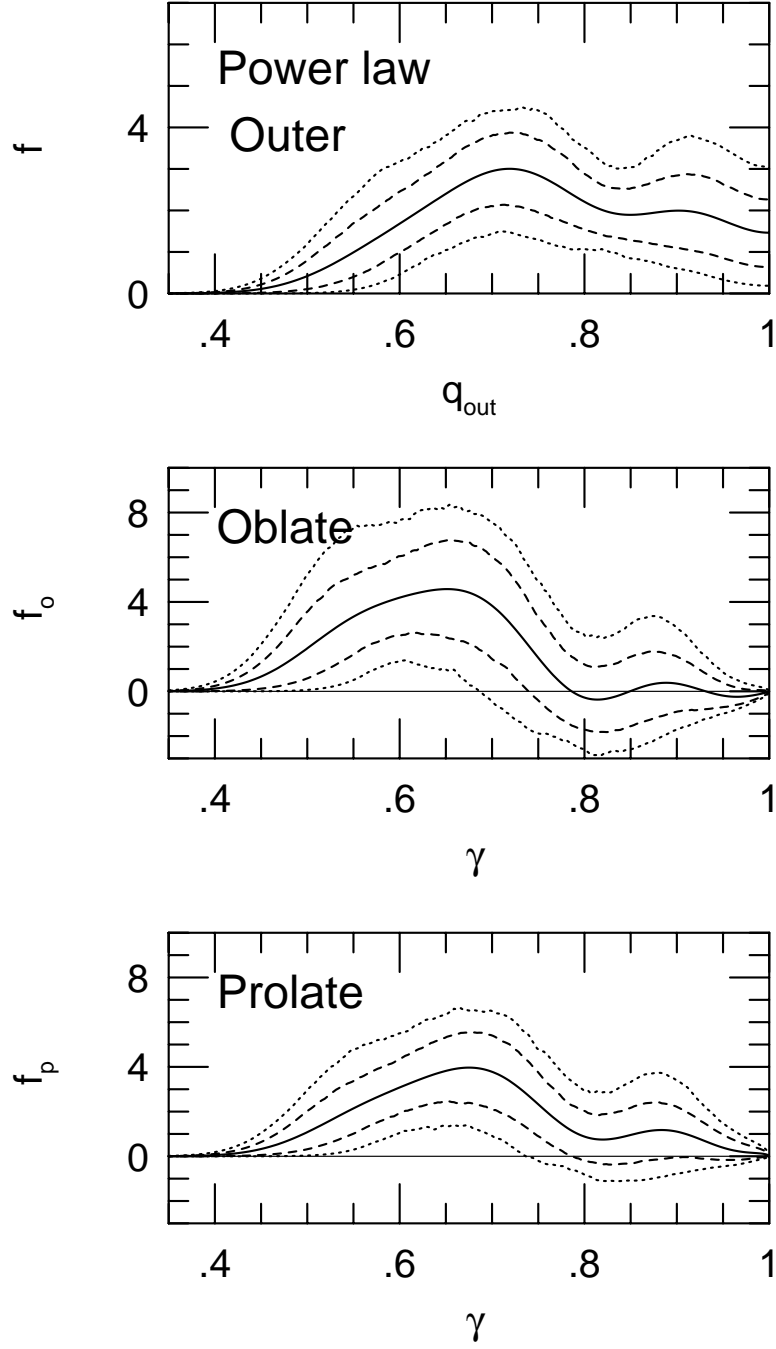


Fig. 7.— As Fig. 2, but for the $t_{\text{dyn}} = 50$ Myr isophotes of the power law galaxies. The sample contains $N = 14$ galaxies; the kernel width is $h = 0.061$.

TABLE 1
APPARENT AXIS RATIOS OF CORE GALAXIES

Galaxy	Distance [Mpc]	r_{in} [arcsec]	q_{in}	r_{out} [arcsec]	q_{out}	Inner isophotes	Outer isophotes
Abell 1020	243.8	0.16	0.915	9.7	0.922	L95	L99
Abell 1831	280.9	0.17	0.905	8.7	0.802	L95	L99
Abell 2052	132.0	0.32	0.738	16.0	0.727	L95	L99
NGC 720	22.6	1.13	0.897	99.3	0.555	L95	P90
NGC 1399	17.9	2.72	0.902	125.	0.912	L95	C94
NGC 1400	21.5	1.41	0.908	L95	L85
NGC 1600	50.2	1.22	0.627	65.5	0.730	L99	P90
NGC 2832	90.2	0.62	0.893	35.1	0.688	L95	P90
NGC 3379	9.9	3.01	0.864	143.	0.843	L99	P90
NGC 3608	20.3	1.35	0.834	65.8	0.809	L95	G94
NGC 4168	36.4	0.80	0.676	51.7	0.855	V94	C90
NGC 4365	22.0	1.97	0.710	110.	0.766	V94	C94
NGC 4472	15.3	2.70	0.914	207.	0.786	V94	C94
NGC 4486	15.3	2.26	0.978	193.	0.785	L92	C90
NGC 4486B	15.3	1.74	0.828	L95	...
NGC 4552	15.3	2.42	0.941	110.	0.877	L99	C90
NGC 4636	15.3	1.04	0.943	132.	0.738	L95	P90
NGC 4649	15.3	2.59	0.947	172.	0.767	L99	P90
NGC 4874	93.3	0.68	0.886	27.5	0.907	L95	P90
NGC 4889	93.3	0.74	0.903	35.8	0.661	L95	P90
NGC 5813	28.3	1.30	0.920	73.4	0.727	L95	P90
NGC 6166	112.5	0.61	0.867	25.6	0.736	L95	L99

TABLE 2
APPARENT AXIS RATIOS OF POWER LAW GALAXIES

Galaxy	Distance [Mpc]	r_{in} [arcsec]	q_{in}	r_{out} [arcsec]	q_{out}	Inner isophotes	Outer isophotes
NGC 221	0.8	14.3	0.737	L98	P93
NGC 596	21.2	1.46	0.922	L95	G94
NGC 1172	29.8	0.90	0.839	40.7	0.726	L95	C88
NGC 1426	21.5	1.20	0.694	60.5	0.646	L95	C88
NGC 1700	35.5	1.33	0.739	60.0	0.683	L95	C88
NGC 2636	33.5	0.46	0.955	L95	...
NGC 3377	9.9	3.18	0.422	97.5	0.607	L95	P90
NGC 3605	20.3	0.70	0.747	L95	P90
NGC 4387	15.3	0.78	0.754	53.1	0.732	L95	C90
NGC 4434	15.3	1.02	0.934	49.0	0.910	L95	C90
NGC 4458	15.3	1.23	0.717	41.6	0.935	L95	C90
NGC 4464	15.3	1.32	0.645	42.0	0.889	L95	C90
NGC 4467	15.3	0.77	0.633	L95	...
NGC 4478	15.3	1.31	0.689	66.4	0.924	V94	C90
NGC 4551	15.3	0.91	0.675	55.3	0.762	L95	C90
NGC 4564	15.3	2.07	0.703	95.2	0.562	V94	C90
NGC 4621	15.3	3.01	0.618	123.	0.752	L99	C90
NGC 4697	10.5	3.02	0.593	158.	0.689	L95	P90
NGC 5845	28.2	1.35	0.691	41.2	0.807	L95	R94
VCC 1199	15.3	0.43	0.692	L95	...
VCC 1440	15.3	0.42	0.902	L95	...
VCC 1627	15.3	0.42	0.844	L95	...

TABLE 3
 KOLMOGOROV-SMIRNOV PROBABILITIES:
 COMPARISON OF ISOPHOTE AXIS RATIOS

		q_{out} (Core)	q_{in} (Power law)	q_{out} (Power law)
q_{in}	(Core)	0.0059	0.0029	0.016
q_{out}	(Core)	...	0.076	0.55
q_{in}	(Power law)	0.92